Experimental Study of the Rate of Bond Formation Betwwen Individual Receptor-Coated Spheres and Ligand-Bearing Surfaces

Anne Pierres, Anne-Marie Benoliel, Pierre Bongrand

Experimental Study of the Rate of Bond Formation Between Individual Receptor-Coated Spheres and Ligand-Bearing Surfaces

Anne Pierres, Anne-Marie Benoliel and Pierre Bongrand (*)

Laboratoire d'Immunologie, INSERM (**), Hôpital de Sainte-Marguerite, B.P. 29, 13277 Marseille Cedex 09, France

(Received 7 February 1996, revised 21 March 1996, accepted 22 March 1996)

PACS.87.15.Kg – Molecular interactions
PACS.87.45.Ft – Rheology of body fluids
PACS.87.22.Bt – Membrane and subcellular physics and structure

Abstract. — The efficiency of cell adhesion is highly dependent on the rate of association between adhesion molecules when membranes are at bonding distance. Whereas kinetic parameters of interactions involving at least one soluble molecular species have been extensively studied, the definition and experimental determination of corresponding parameters when both receptors and ligands are bound to surfaces are much more difficult to achieve. In the present work, we explore the feasibility of measuring the rate of association between antibody-coated spheres and antigen-derivatized surfaces in presence of an hydrodynamic shear force lower than the strength of a single bond. An image analysis procedure allows continuous recording of particle position with about 0.05 μm accuracy and a time resolution of 5 milliseconds. We present an original procedure allowing direct determination of the wall shear rate by processing the images of moving spheres. Further, simultaneous determination of the Brownian fluctuations perpendicular to the bulk fluid motion and the mean translational velocity of particles allows in principle a numerical determination of the sphere-to-substrate distance within a range of about 10 to 1000 nm. It is concluded that: i) particle motion is in rough agreement with current hydrodynamic theories based on creeping flow approximation. ii) In our experimental system, adhesion seems to be diffusion-limited, therefore, only a lower boundary for the kinetic constant of molecular association can be obtained. iii) Further improvement of our method will require the production of molecularly smooth receptor-coated surfaces.

1. Introduction

Many important cellular processes such as migration, differentiation, proliferation or immune recognition are critically dependent on adhesive events. These phenomena involve the formation and dissociation of specific bonds between membrane molecules. Adhesion efficiency is therefore highly dependent on the kinetic properties of these interactions. Indeed, when a first bond is formed between a cell and a surface, the outcome of the encounter is dependent on the ratio between the lifetime of the first bond and the time required for the formation of

(*) Author for correspondence (e-mail: bongrand@ infobiogen.fr)
(**) U 387

additional links. An important example is the adhesion of flowing leukocytes to blood vessels during inflammatory reactions: the initial interaction results in dramatic decrease of the flowing velocity of leukocytes touching endothelial cells. This phenomenon is called rolling and is mediated by transient associations between selectins and mucin-like molecules [1,2] or integrins and molecules of the immunoglobulin superfamily (3). It was postulated that rolling required particularly high constants of association and dissociation between interacting molecules [2,4]. Final adhesion would then require the interplay of other ligand and receptor couples, with lower kinetic constants.

Much theoretical work was done to account for these phenomena. In a seminal paper, George Bell [5] built a framework to model cell adhesion. He suggested a simple way of relating interactions between free molecules and associations between surface-bound structures by considering bond formation as a two-step reaction, including diffusion-mediated formation of an encounter complex and molecular bonding. The kinetics of formation of the encounter complex was calculated by neglecting the relative motion of interacting surfaces that were assumed to remain at bonding distance.

Many authors elaborated on Bell's model in order to achieve quantitative predictions concerning the equilibrium contact area of interacting cells [6], force required to separate bound cells [7], kinetics of cell attachment [8] and detachment [9], modelling of the rolling phenomenon [10,11]. Further, several authors emphasized the expected peculiarities of interactions mediated by a very low number of ligand receptor bonds [12,13]. Since all these models made use of unknown bonding parameters, there was an increasing need to obtain reliable experimental data on the properties of individual bond formation and dissociation involving surface-bound molecules. However, available techniques have long allowed to study only interactions involving at least one soluble molecular species [14,15].

A possible way of approaching this goal consisted of studying the motion of receptor-bearing particles subjected to a laminar shear flow near a planar ligand-derivatized surface. The simplest approach consisted of counting the fraction of bound particles. However, precise interpretation of numerical results required a precise knowledge of the conditions of contact between particles and substrate. Substantial progress could be obtained by studying adhesion at the single particle level. Indeed, bond formation may be easily monitored by studying discontinuities of particle velocity. Also, the distance between flowing particles and the surface may be estimated by means of theoretical results of fluid mechanics relating the translational velocity U of a sphere near a surface to the wall shear rate G and sphere radius a [16–18]. Indeed, when the width δ of the gap between the sphere and the wall becomes vanishingly small, the ratio U/aG roughly decreases as the inverse of $\ln(\delta/a)$, allowing quantitative estimate of δ over a fairly wide range of orders of magnitude. This approach allowed quantitative check of the double layer theory in order to account for the interactions between colloidal particles and flat plates [19].

Many experimental models of cell-surface adhesion under flow were reported, including nonspecific interactions between glass surfaces and tumor cells [20], neutrophils [21] or macrophage-like cells [22], adhesion between receptor-bearing surfaces and cells [2, 23–26] or artificial particles such as liposomes [27] or latex beads [28], and fixation of flowing cells to cell monolayers (*e.g.* Refs. [29,30]). An interesting approach consisted of studying the nonspecific or antibody-mediated adhesion of hypotonically sphered red cells to glass surfaces under controlled conditions of flow [31]. Several consistent findings may be emphasized:

i) The probability of cell adhesion per unit length of trajectory seems inversely related to the shear rate [24, 25] and also to the cell velocity for a given shear rate [30]. However, different results might be obtained with model particles [28].

ii) The width of the cell substrate gap deduced from the cell velocity in a flow chamber is often much higher (say about 100 nm or more) than the sum of the lengths of ligand and receptor molecules [23,31]. However, the relevance of standard models of fluid mechanics to short-distance interactions between actual cells and flat surfaces was questioned [31,32].

iii) No substantial decrease of cell velocity was detected immediately before adhesion [20,23].

The aim of the present work was to study the initial adhesive event in a flow chamber with improved accuracy. First, flowing particles were artificial spheres. Indeed, in addition to aforementioned problems concerning the relevance of fluid mechanic theory to actual cells [33], the motion of biological cells is too irregular to allow objective detection of very short arrests [34]. Second, the position of spheres was determined with an image analysis procedure allowing better than 0.1 μm accuracy [35]. Third, the motion was recorded with a rapid videocamera allowing 5 millisecond temporal resolution. Fourth, an original procedure was developed in order to allow quantitative derivation of the wall shear rate from observed images. Fifth, we described a new method based on Brownian motion analysis for testing the hydrodynamic theory of sphere displacement near a surface in laminar shear flow. Particles were latex beads coated with limiting amounts of anti-rabbit immunoglobulin antibodies, and the surface was derivatized with rabbit immunoglobulins [28]. This system allowed direct experimental study of the influence of particle velocity and distance to the surface on binding efficiency. It is concluded that our approach may give direct information on the rate of bond formation between surface-bound receptors and ligands.

2. Materials and Methods

2.1. PARTICLES AND SURFACES. — Our system was fully described in a previous report [28]. Briefly, particles were spheres of 2.8 μm diameter and 1.3 g l^{-1} density (Dynabeads M280, Dynal France, Compiègne) derivatized with streptavidin, a high affinity receptor for biotin. They were coated with biotinylated anti-rabbit immunoglobulin murine monoclonal antibodies (IgG2a, clone IgL 173, Immunotech, Marseille) diluted at 1/1,000 and 1/5,000 in irrelevant antibodies of similar class and species (anti-CD14, clone UCHM1, Sigma France, St. Quentin-Fallavier). The densities of binding sites were respectively estimated at about 3.5 and 0.7 molecules per squared micrometer [28].

Glass surfaces were coated with 1 mg ml^{-1} polylysine (Sigma, MW > 300,000), then treated with 2,4 dinitrobenzenesulfonic acid (Eastman Kodak, Rochester, NY) and coated with rabbit anti-dinitrophenyl antibodies (Sigma) as previously described [28]. The achieved surface density was about 6,200 molecules μm^{-2}

2.2. FLOW CHAMBER. — We used a modification of a previously described apparatus [28,33]. The chamber was a rectangular cavity of $6 \times 17 \times 0.16$ mm^3 made out of a drilled plexiglas block and a glass coverslip. The inlet and outlet were pipes of 1 mm inner diameter. Immunoglobulin-coated glass coverslips were stuck on the bottom with silicon glue. The chamber was set on the stage of an inverted microscope (Zeiss Axiovert 135) using a 40X lens (Achroplan, 0.65 NA). T he flow was generated by a 1 ml syringe mounted on a syringe holder with adjustable velocity (Razel, supplied by Bioblock, Ilkirch, France). The wall shear rate G could be calculated with a standard formula [2,23,31]:

$$G = 6Q/wh^2 \tag{1}$$

where Q is the flow rate, and w and h are the chamber width and height respectively.

The microscope was connected to a LHR 712 rapid video system (Lhesa, Cergy-Pontoise, France) consisting of a CCD camera and a modified Panasonic videotape recorder yielding 100 full format frames per second and up to 800 frames per second with reduced format. Under standard conditions, half format images were recorded with a rate of 200 frames per second and videotapes were used to obtain a standard (video-rate) output for delayed analysis. The video signal was processed with a PCVision+ real time digitizer (Imaging Technology, Bedford, MA, supplied by Imasys, Suresnes, France) yielding 512 × 512 pixel images with 256 gray levels. This was mounted on a standard desk microcomputer (a 80486 microprocessor with 25 MHz frequency was sufficient). The pixel size was obtained by measuring the grid of a Neubauer hemocytometer: this was found to be 0.24 and 0.17 μm along directions respectively parallel (x-axis) and perpendicular (y-axis) to the sphere motion.

2.3. Position Determination and Image Analysis. — Real time accurate determination of particle position was performed with a custom-made assembly-language software developed in the laboratory. The principle was as follows. The microscope was focussed in order that beads appeared as bright discs surrounded by a thick black area. A vertical line was continuously scanned on the side of the field. When the passage of a dark object was detected, a small (32 × 32 pixel) image surrounding this object was transferred into the computer memory (transferring one every two pixel, thus resulting in twofold decrease of particle size and separation of odd and even frames in an interlaced image). The particle was located with a boundary-follow procedure based on intensity threshold [34]. It was then possible to record the object area and coordinates of the center of gravity. As will be shown below, the area recording allowed easy detection of interactions between two particles that might artefactually simulate binding events.

In order to estimate the vertical position of the beads with micrometer accuracy, images were processed by determining the radial brightness distribution with sequential steps of 0.2 μm. The intensity distribution could be empirically related to the apparent distance between particles and the focus plane by proper calibration: the distance between particles and the microscope objective was varied by steps of 1 or 2 μm with the micrometer controlling the microscope stage. Then, sequential images of a given bead were analyzed. Results were used to derive the apparent distance between the objective and flowing beads. The actual distance was estimated by multiplying this apparent distance with the refractive index of water (*i.e.* 1.33).

2.4. Analysis of Motion and Arrests. — The motion of 709 individual particles was followed, yielding 216,368 sequential positions. An automatic procedure was therefore needed to define particle arrests. As previously discussed [34], a particle might be considered as arrested if it moved by less than a threshold length L during a given time interval T. The determination of L and T required some arbitrariness, which is a major problem when one aims at determining the influence of cell velocity on arrest frequency. After visual examination of all 709 trajectories, the following procedure was found convenient:

- First, by examining the position of arrested particles during hundreds of sequential steps. if was found that the *maximum amplitude* of variation of positions was about 0.5 μm (*i.e.* 2. pixels - note that the *standard deviation* of the measured x coordinate of arrested particles was about eightfold lower, *i.e.* less than 0.1 μm). A particle could thus be considered as arrested when it moved by less than 0.5 μm, which settled parameter L to 2 pixels.
- Parameter T was then determined in each *individual* experiment as follows: the mean velocity V of particles moving in close contact with the surface was easily determined (see histograms in following section). A particle was thus considered as arrested if it moved by less than length

L during a time interval T equal to $4L/V$, corresponding to a velocity fourfold lower than that of the slowest particles with continuous motion. A visual examination of all recorded trajectories suggested that this algorithm allowed straightforward detection of nearly 90% of arrests with essentially no false positive. Only very short-time arrests could be missed, and it was difficult to decide whether these events represented actual arrests or random errors in the determination of particle location.

Binding frequencies were determined as previously described by dividing the total length of monitored trajectories under given conditions by the number of arrests [28.30]. Since particle detection was performed by the computer, no bias related to particle choice was expected.

2.5. BROWNIAN MOTION ANALYSIS. — The diffusion coefficient D_y along an axis parallel to the chamber floor and perpendicular to the motion could in principle be obtained with the well-known formula:

$$\langle \Delta y^2 \rangle_t = 2D_y t \tag{2}$$

where $\langle \Delta y^2 \rangle$ is the mean square displacement along y during time t. When the particle trajectory is not rigorously perpendicular to axis Oy, it may easily be shown that

$$\langle \Delta y^2 \rangle = 2D_y t + v_y^2 t^2 \tag{3}$$

where v_y is the velocity component along axis Oy. Particle trajectories were used to calculate $\langle \Delta y^2 \rangle$ for two values of the time interval (0.08 s and 0.02 s) in order to determine D_y with equation (2).

3. Results

3.1. DIRECT DETERMINATION OF THE WALL SHEAR RATE. — Although the wall shear rate could be easily determined with equation (1), the median particle velocity sometimes displayed significant variations between different experiments where the flow rate was identical. This might be ascribed to unexpected variations of the chamber thickness due to occasional deformation of the coverslip when the chamber was filled. It was therefore felt useful to develop a method allowing quantitative determination of the shear rate on the very same microscopic field that was examined to monitor adhesion. The basic idea was that the image of a bead was sharply dependent on its distance to the focus plane, as shown in Figure 1. Thus, it was conceivable to measure at the same time the velocity and the distance to the wall of beads subjected to hydrodynamic flow in the chamber. This was achieved as follows: in five series of experiments, a microscopic field containing several beads was selected and the stage was moved by steps of 2 μm with concomitant digitization of sequential images. As exemplified in Figure 2, the radial distribution of relative brightness displayed regular changes when the bead positions was varied. It was found convenient to use the relative intensity at 1.1 μm from the center of gravity as a "sharpness parameter" (this was chosen in order to minimize the dependence on the camera settings, due to imperfect linearity of the image analysis system). Calibration curves were then obtained by plotting this sharpness parameter *versus* the bead position. A representative curve is shown in Figure 3. It was thus possible to appreciate the height of flowing spheres with better than micrometer accuracy when this ranged between about 4 and 16 μm.

A flow experiment was then performed, and the translational velocity of flowing beads was determined together with their distance to the chamber floor (note that the microscope had to be focussed below the chamber floor, in order to use the smoothest part of the curve in Fig. 3). The velocity v of individual beads could then be plotted *versus* their vertical coordinate h. As

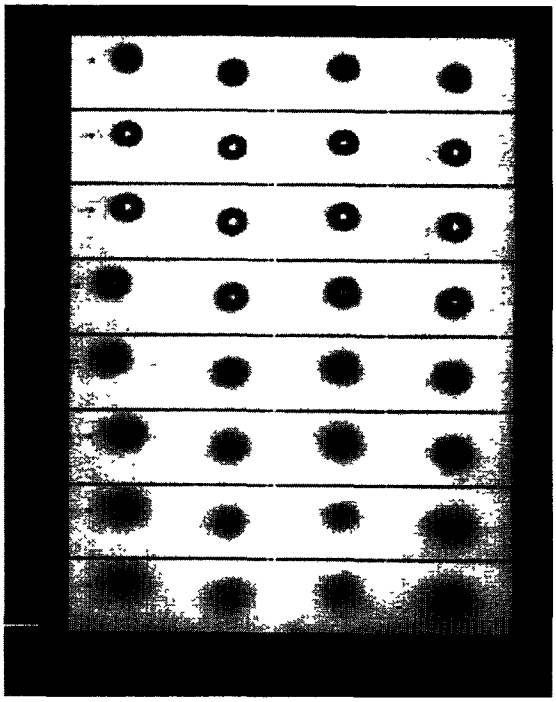

Fig. 1. — Relationship between bead image and distance to focus plane. Spherical beads of 2.8 μm diameter were deposited on a microscope slide in the flow chamber, on a microscope stage. The objective was subjected to sequential vertical displacements of 2 μm while a series of four beads were digitized with subsequent recording of 32 × 32 pixel images surrounding them. Each row displays the set of four images obtained for a given distance to the focus plane. Bar is 5 μm.

shown in Figure 4, when the bead height h was higher than a few micrometers, v was fairly proportional to h, yielding the wall shear rate G as the slope of the regression line.

3.2. Analysis of Particle Trajectories. — The trajectories of individual particles were observed. An example is shown in Figure 5. Clearly, particles moved with fairly regular pace with occasional decrease (A) or increase (B) of this velocity. In some cases, an artifactual velocity change occurred when the particle passed near another one. In this case, the area displayed marked increase (C). Corresponding segments were systematically discarded.

A typical arrest is shown in Figure 6: this was sharp without any progressive velocity decrease which allowed accurate definition of particle velocity before arrest.

3.3. Particle Velocity Distribution. — Since we wished to determine the dependence of arrest frequency on particle velocity, it was of interest to study the distribution of particle velocities. The distribution of velocities per time interval of 40 milliseconds in a representative experiment is shown in Figure 7 (G is 28 s^{-1}). The distribution of mean velocities of individual particles (in absence of arrest) for two values of the shear rate (14 and 28 s^{-1}) is shown in Figure 8. Clearly, there was a sharp frequency maximum corresponding to the population of particles that were in apparent contact with the chamber floor. The distribution was skewed with a rightward shoulder corresponding to incompletely sedimented particles that presumably passed at distance from the surface.

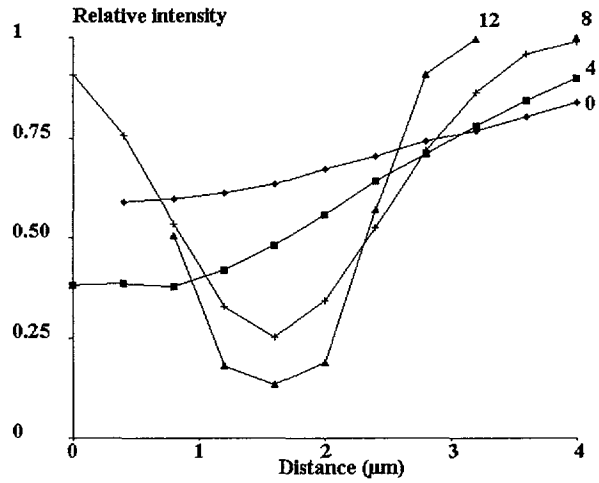

Fig. 2. — Relationship between radial intensity distribution of bead images and distance to focus plane. Digitized bead images obtained as shown in Figure 1 were used to derive the radial intensity distribution. Curves obtained for a bead observed with subsequent displacements of 4 μm of the microscope objective are shown. The initial curve (labelled 0) represents an image obtained when the focus plane is well below the beads. Other numbers indicate the objective upward displacement (in micrometer) from the initial position.

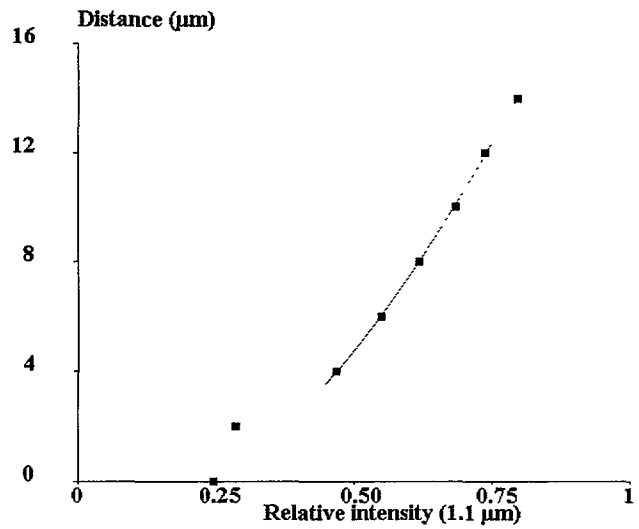

Fig. 3. — Use of digitized bead images to determine the distance to the focus plane. Series of 4 to 8 spherical beads were examined at different distances d from the microscope focus plane, and the mean relative brightness at 1.1 μm distance from their center of gravity was calculated. This mean was plotted *versus* d. The standard error of the mean ranged between 0.005 and 0.01. Note that the region where the distance to the focus plane ranges between about 4 and 16 μm is well described by a segment of a parabola.

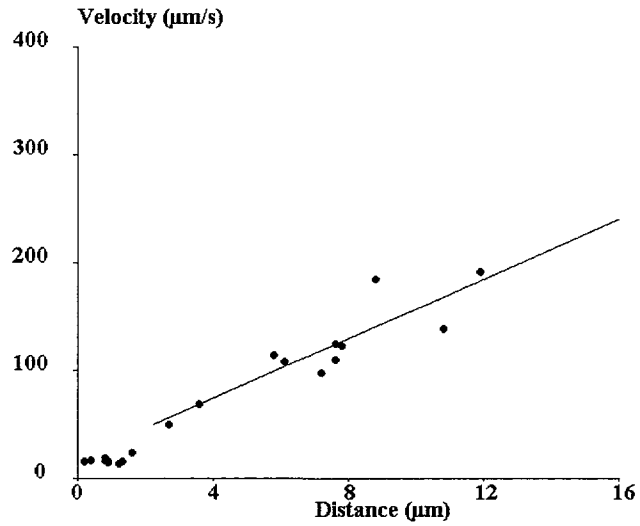

Fig. 4. — Dependence of bead velocity on distance to the focus plane. Spherical beads were subjected to hydrodynamic flow and monitored microscopically. The focus plane was about 2 μm below the flow chamber. The vertical coordinate was estimated with a calibration curve as shown in Figure 3. The translation velocity was determined by sequential determination of the center of gravity. Values obtained with 18 particles observed in the same experiment are shown. The wall shear rate was derived from the slope of the regression line obtained with cells that were higher than the chamber floor by about 4 μm or more.

3.4. Dependence of Arrest Frequency on Bead Treatment. — Since there is always a possibility that particle arrest be due to nonspecific interactions with the chamber floor, the relative concentration of specific anti-rabbit antibodies on the beads was varied and the arrest frequency was determined. As shown in Table I, increasing specific antibody concentration from 1/5,000 to 1/1,000 markedly increased the arrest frequency, whereas beads coated with 1/5,000 specific antibodies or controls displayed essentially similar behavior. Therefore, we used beads coated with 1/1,000 specific antibodies as a convenient model since, i) most arrests were presumably due to specific interactions and ii) it was possible to follow the motion of particles in close contact with the substratum for sufficiently long periods of time.

3.5. Dependence of Arrest Frequency on Particle Velocity. — An interesting finding appearing in Table I is that when the shear rate was increased, the frequency of specific arrests *per unit of time* was increased whereas the arrest frequency per micrometer remained essentially unaltered. However, as shown in Table II, when the arrest frequency of particles with different velocities *for a same shear rate* was studied, even a slight velocity increase (in the order of 25%) resulted in marked decrease of arrest frequency (about 2- to 3-fold per micrometer).

However, data interpretation raised an important problem: particle velocities used to build Tables I and II were mean velocities calculated on the *entire trajectory* preceding arrest. This seemed a reasonable choice when arrest frequencies had to be estimated. However, discussing the mechanism of cell binding required an knowledge of the particle velocity *immediately before arrest.* Therefore, both parameters were compared: as shown in Figure 9, there was a fairly strong correlation between non dimensional velocity (*i.e.* U/aG) along entire trajectories and

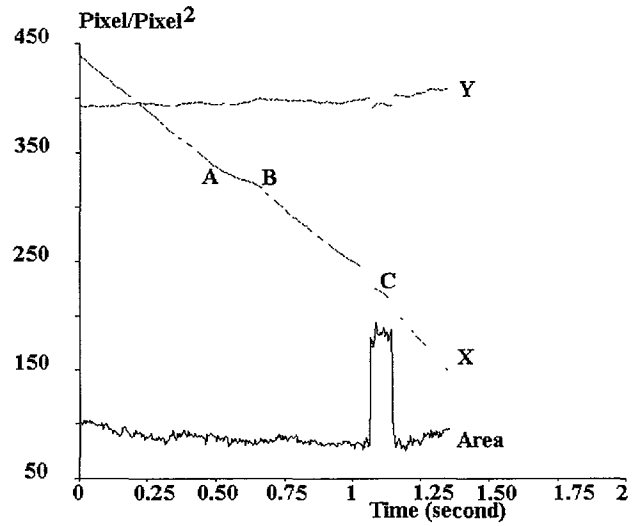

Fig. 5. — Automatic monitoring of particle trajectories. The motion of flowing beads was recorded on a rapid video-system. The videotape was replayed in order to obtain a standard video-signal that was subjected to real-time analysis with determination of particle coordinates (x-axis is parallel to the chamber axis and y-axis is perpendicular to the average motion) and particle area. The velocity is fairly constant on periods of time separated by sudden decrease (A) or increase (B) of this velocity. When a slower particle was caught up with a more rapid particle (C), interaction appeared as a transient area increase, corresponding to the temporary replacement of a sphere with a doublet.

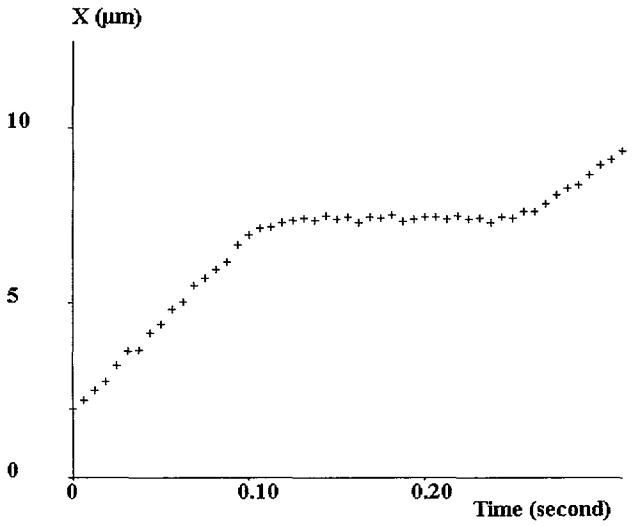

Fig. 6. — Typical trajectory and arrest. A typical particle trajectory is shown by plotting the x coordinate *versus* time. Typical arrests were not preceded by progressive slow down, as shown on a representative example.

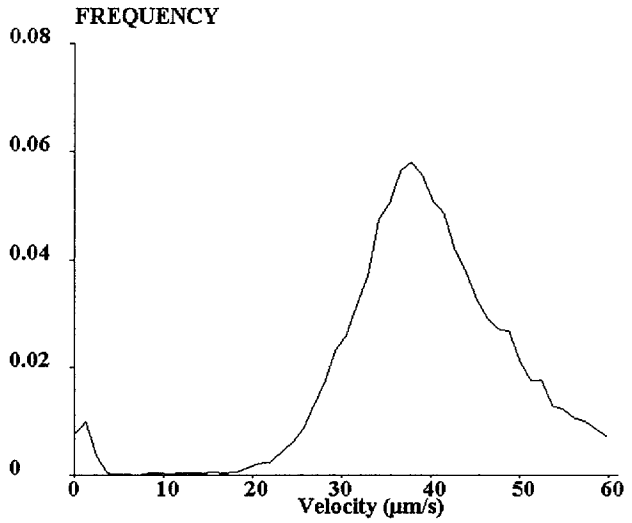

Fig. 7. — Distribution of instantaneous velocities. In a representative experiment, the motion of 45 particles were followed during part or totality of their passage through the microscope field. Positions were determined every 0.005 s, yielding a total of 17 129 positions. The mean velocity was determined on each sequence of 8 elementary steps (*i.e.* 40 millisecond interval) and the frequency distribution of these intervals is shown. The leftward peak corresponds to arrested particles. The major peak corresponds to moving particles. The wall shear rate is 28 s^{-1}

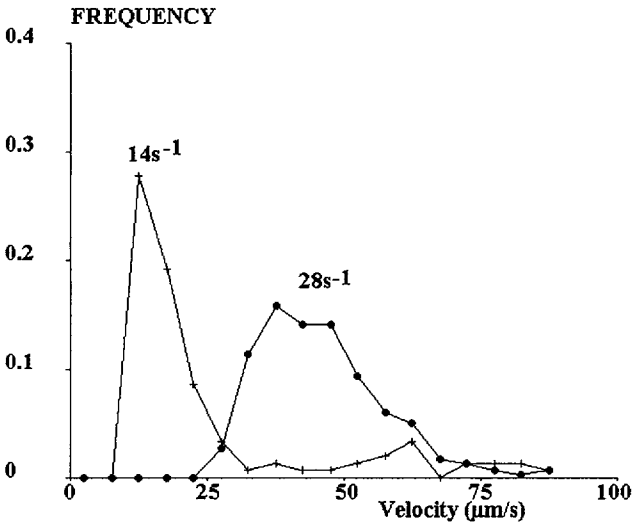

Fig. 8. — Distribution of individual particle velocities. The mean velocity of flowing particles was determined during their passage across the microscope field, using segments excluding arrests. The frequency distribution of mean particle velocities are shown for two values of the wall shear rate (14 s^{-1} and 28 s^{-1}). A total of about 500 trajectories were used.

Table I. — *Effect of shear rate and antibody concentration on arrest frequency. Beads of radius $a = 1.4$ μm were coated with different concentrations of anti-rabbit immunoglobulin antibodies (0, 1/5,000 and 1/1,000) and driven against a surface coated with rabbit immunoglobulin, with two different values of the wall shear rate G. Individual particles were followed for determination of mean velocity U and detection of arrest events. Only beads with a ratio U/aG lower than 1.25 were followed for the determination of arrest frequency per length and time unit.*

Wall shear rate (s^{-1})	Ab dilution	Mean $\langle U/aG \rangle$	Total time (s)	Total distance (μm)	Arrest frequency (μm^{-1})	s^{-1}
14	∞	0.80	133.2	2090.3	0.0053	0.083
14	5,000	0.65	58.4	742.6	0.0013	0.017
14	1,000	0.71	235.8	2596.9	0.0092	0.102
28	∞	0.94	89.1	3216.5	0.0019	0.067
28	5,000	1.15	58.3	2640.4	0.0019	0.086
28	1,000	0.66	58.7	1182.4	0.0085	0.170

Table II. — *Effect of individual particle velocity on arrest frequency. Beads of radius $a = 1.4$ μm coated with 1/1,000 anti-rabbit immunoglobulin antibodies and driven against a surface coated with rabbit immunoglobulin, with two different values of the wall shear rate G. Individual particles were followed for determination of mean velocity U and detection of arrest events. Only beads with a ratio U/aG lower than 1.25 were studied. The influence of individual particle velocity on arrest frequency is shown.*

Wall shear rate (s^{-1})	$\langle U/aG \rangle$		Total time (s)	Total distance (μm)	Arrest frequency (μm^{-1})	(s^{-1})
	Range	Mean				
14	[0.36-0.67]	0.56	103.8	915.2	0.0131	0.116
14	[0.68,1.25]	0.82	129.7	1637.2	0.0073	0.093
28	[0.20,0.57]	0.51	16.6	274.3	0.0182	0.301
28	[0.58,1.12]	0.72	42.2	908.1	0.0055	0.118

immediately before arrest, the latter value being lower than the former by about 25%. Also, arrest events were observed on particles with fairly different values of parameter U/aG.

3.6. Particles Display Typical Brownian Motion. — Since the above results suggested that in some cases particles located at a substantial distance from the substratum might become bound, the importance of fluctuations of particle position was considered. It was therefore felt interesting to compare the fluctuations of particle position to values expected from Brownian motion theory. This question was addressed by calculating the mean squared variations of coordinates x (parallel to the motion) and y (perpendicular) on a set of particles. A typical set of results is shown in Figure 10: whereas $\langle \Delta x^2 \rangle$ was fairly proportional to the square of time, as expected for a motion with uniform velocity, $\langle \Delta y^2 \rangle$ was fairly proportional to the first power of time intervals, as expected from typical Brownian motion. When the particle was bound, $\langle \Delta x^2 \rangle$ and $\langle \Delta y^2 \rangle$ were essentially independent of time, yielding an estimate of the accuracy of position determination.

In order to make these conclusions more quantitative, 38 different particle trajectories were analysed for determination of the diffusion coefficient D_y perpendicular to the motion. A plot

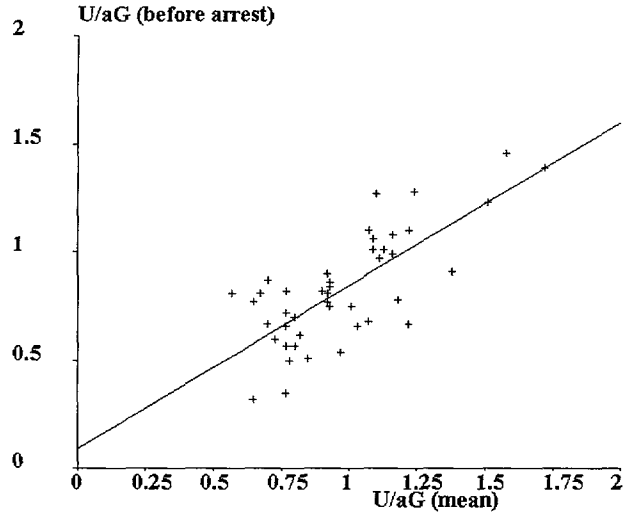

Fig. 9. — Variation of cell velocity before arrest. The trajectories of 45 particles displaying an arrest during their passage through the microscope field were used to determine the mean velocity U on the whole trajectory preceding arrest (abscissa) and during the last 40 milliseconds preceding arrest (ordinate). Dimensionless values (U/aG) are shown together with the regression line (the correlation coefficient is 0.747, the slope is 0.753).

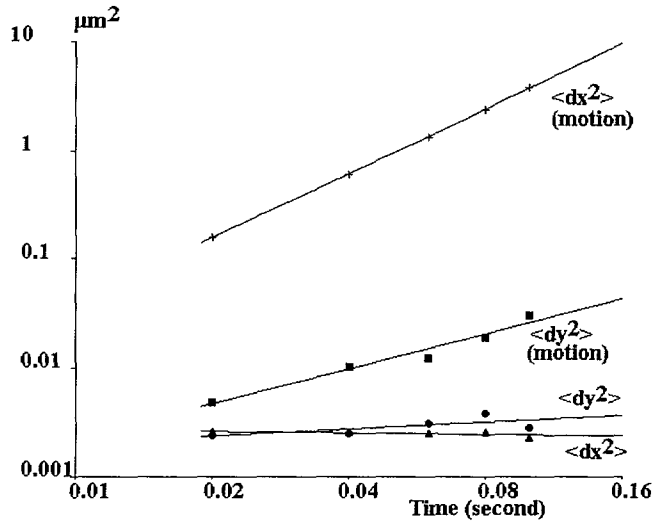

Fig. 10. — Study of Brownian motion on a typical particle. The trajectory of a typical particle displaying a long-term arrest was used to calculate the mean square variations of coordinates x and y (respectively parallel and perpendicular to the motion) during variable time intervals (between 0.02 and 0.16 s), either during motion (crosses and squares) or during arrest (circles and triangles). Experimental values are displayed on a log-log plot together with regression lines. The slope of the regression lines of $\log\langle dx^2\rangle$ and $\log\langle dy^2\rangle$ plotted *versus* $\log(t)$ are 1.9777 and 1.0702 respectively.

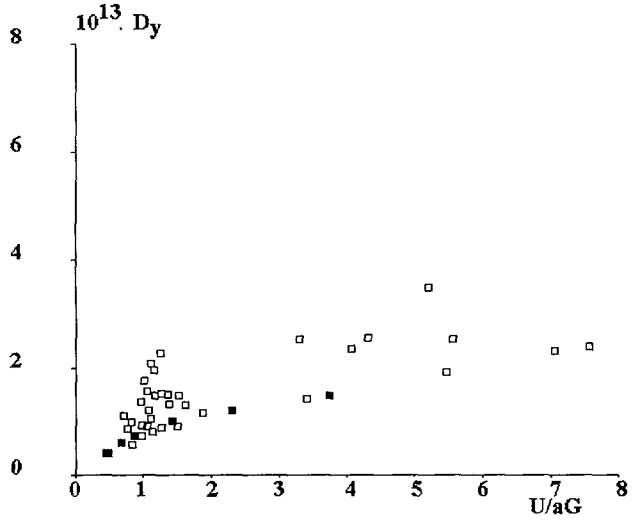

Fig. 11. — Relationship between horizontal diffusion coefficient and relative particle velocity. The trajectories of 24 individual particles were used for simultaneous determination of diffusion coefficient for lateral displacements and dimensionless velocity U/aG. Empty squares represent experimental data. Full squares were derived with theoretical results from fluid mechanics [15, 34].

of D_y *versus* U/aG is shown in Figure 11 together with a theoretical plot based on numerical values of the friction coefficient of a sphere moving along a plane wall in viscous fluid [37]. Since experimental errors of position determination might yield artefactually increased values of D_y, it was attempted to estimate these errors by performing a similar analysis on arrested particles: analysis of 10 trajectories yielded a mean value of 0.43×10^{-13} m^2 s^{-1} (corresponding to a mean square displacement of 4.3×10^{-4} μm^2 during 0.02 second intervals).

4. Discussion

Our ultimate goal was to obtain direct information of the rate of association between adhesion molecules bound to surfaces separated by a gap of known width. The basic idea was to observe the motion of receptor-coated spheres driven along ligand-derivatized surfaces in presence of a hydrodynamic force much lower than the expected strength of a single molecular bond [6, 38–40]. It was thus expected that first, bond formation would result in detectable particle arrests and second, that the measurement of particle velocity might give precise information on the distance between particles and surfaces. The performance we achieved benefitted from combined use of accurate determination of particle position (better than 0.1 μm), high temporal resolution (5 milliseconds) and automated processing of numerous particle positions (more than 200,000). Note that the possibility of achieving high accuracy measurement of particle location by determining the centroid of microscopical images was reported by Uyeda *et al.* [42] who located actin molecules with a resolution of about 14 nm.

Our experimental findings were as follows:

i) Spheres moved across the microscope field with fairly constant velocity. The velocities

of different particles displayed substantial differences, presumably depending on the distance between these particles and the chamber floor.

ii) Flowing spheres exhibited occasional sudden arrests, without detectable velocity decrease during the preceding 0.04 second.

iii) When the shear rate was increased by a factor two, the number of arrests detected per unit of particle displacement length was not substantially altered, suggesting that the limiting parameter for adhesion might be the frequency of flow-driven encounters between receptors and ligands.

iv) For a given shear rate, more rapid particles exhibited much rarer arrests than slower ones, in accordance with the hypothesis that they were more distant from the surface. However, the velocities of particles that displayed at least one arrest varied by a factor higher than two.

Several questions must be answered in order to achieve full interpretation of these results.

4.1. What is the Actual Distance Between Particles and Surface Before Arrests? — As shown in Figure 9, the mean velocity of most stopping particles ranged between about 0.4 aG and 1.5 aG with occasional higher values during the 40 ms preceding arrest. Following Goldman and colleagues [19], the corresponding width of the particle-to-surface gap would thus range between $0.001 \times a$ and $0.2 \times a$, *i.e.* between 1.4 and 700 nm. Since the latter value is at least twentyfold higher than the sum of lengths of two immunoglobulin G molecules [41], if we assume that the hydrodynamic theory is actually relevant to artificial spheres (see the discussion by Hammer, [32]), two possible nonexclusive interpretations of our results is that *at least in some cases* contact occured through local protrusions of particles or surface [33] or transient fluctuations of particle-to-surface distance ([23], see below for further discussion of these fluctuations).

4.2. Are the Estimated Values of Diffusion Constants Consistent with Velocity Determinations? — Interestingly, quantitative determination of lateral Brownian fluctuations (*i.e.* perpendicular to the motion) might give direct information on the distance between moving spheres and the surface without requiring any knowledge of the shear rate. Let us consider the particles with lowest U/aG in Figure 11: the estimated diffusion coefficient is 1.16×10^{-13} m^2 s^{-1}. However, if we subtract the contribution of measurements errors (estimated at 0.43×10^{-13} m^2 s^{-1}), the corrected value of D_y is 0.72×10^{-13} m^2 s^{-1}. Using Einstein's relationship between the diffusion coefficient D and the friction constant f together with Stoke's formula for f, we obtain for the undisturbed diffusion coefficient at distance from the wall:

$$D_{y_0} = kT/f = kT/6\pi\mu a = 1.57 \times 10^{-13} \text{ m}^2 \text{ s}^{-1} \tag{4}$$

where μ is the medium viscosity (10^{-3} Pa $\times$ second for water), k is Boltzmann's constant and T the absolute temperature. Thus, the diffusion coefficient is reduced by a factor of 2.18 (1.57/0.72) for the slowest spheres. The corresponding dimensionless particle-to-surface distance is about 0.12 [37], *i.e.* about 170 nm with a value of 0.86 for U/aG [17].

Note that the more rapid particles exhibited a diffusion coefficient *higher* than the theoretical value. This may be ascribed to nonthermal fluctuations of position, perhaps as a consequence of local irregularities of the substratum with subsequent perturbation of the flow.

Thus, the values of longitudinal velocities and lateral fluctuations may be considered as consistent provided we accept variations of about 15% in the local shear rate or uncontrolled perturbation of lateral fluctuations by surface irregularities of particles and substratum.

4.3. What are the Expected Properties of Vertical Fluctuations of Sphere Position? — First, let us assume that nonspecific repulsion between flowing particles and the surface may be approximated as a hard barrier. From Boltzmann's law, the probability of

finding the sphere at distance z from the barrier is:

$$P(z) = \exp(-4/3\pi a^3(\rho - \rho_0)gz/kT) \tag{5}$$

where ρ and ρ_0 are the densities of spheres (1.3 kg m^{-3}) and water, and g is 9.81 m s^{-2} By straightforward integration, the mean value of z is:

$$\langle z \rangle = 3kT/[4\pi a^3(\rho - \rho_0)g] = 122 \text{ nm} \tag{6}$$

This value is much higher than the expected range of nonspecific repulsions [43] and it seems sufficient to account for the relatively high mean value of particle velocities, together with incomplete sedimentation.

Another important point is the timescale of these fluctuations. The important point is that, as shown by Brenner [16], the motion of a sphere perpendicularly to a plane surface may be considerably decreased by viscous effects near the plane. Thus, when the dimensionless gap δ/a is about 0.12 as estimated from Brownian motion, the "vertical" diffusion coefficient is 9.25 times lower than the "free" value. Further, using equation (2.19) of reference [14], it is found that D may be lower than 1/100 the free value when δ/a ranges between 0.05 and 0.1. Thus, the time $L^2/2D$ required for a particle height to fluctuate by 10 nm may range between about 3 and 30 milliseconds. Therefore, some arrests must have involved an interaction between protrusions on the surface of particles and/or substratum.

4.4. Significance of the Measured Arrest Frequency. — When particles of velocity U and radius a are close to the chamber floor, their rotational velocity is about $U/2a$ [17]. Therefore, the relative velocity of receptors on the particle surface and the chamber floor is of order $U/2$. Assuming that we have a large excess of binding sites on the substrate and defining λ as the width of the region scanned by a single receptor on particles, the expected number of encounters between a particle-bound antibody and antigen sites when the particle has moved by a length L while remaining within binding distance, is $(L/2)\lambda$ times the surface density of antibody sites. When antibody dilution is 1/1,000, the site density σ is 3.5 molecules per μm^2. Using a tentative value of 10 nm for λ (corresponding to the *order of magnitude* of the length of antibody molecules) we obtain a collision frequency of about $\lambda \times (U/2) \times \sigma = 0.35$ s^{-1} for a particle of 20 μm s^{-1} translational velocity. This is quite close to the values shown in Table II, suggesting that the binding reaction is diffusion-limited. This sets a lower limit to the kinetics of bond formation between surface-bound antigen and antibodies. Indeed, assuming an interaction range of about 10 nm, the collision time for a particle of 20 μm s^{-1} velocity is in the order of 0.001 second (*i.e.* 10 nm/[20 μm^2 s^{-1}]). Note that this conclusion is in line with previous findings by Xia *et al.* [31] who studied the adhesion of immunoglobulin-coated red cells to antigen-coated glass surfaces.

4.5. Conclusion and Perspectives. — The above study demonstrated the feasibility of monitoring the motion of receptor-coated spheres along ligand-derivatized surfaces with 0.1 μm accuracy and 0.005 second temporal resolution. Results are consistent with the hypothesis that, i) standard results of hydrodynamic theory satisfactorily account for sphere motion, ii) thermal motion and substrate roughness probably play a more important role than nonspecific repulsion in determining particle-to-surface interaction in our model, and iii) the time required for association between surface-bound antigen and antibodies is less than 0.001 second in our system

Clearly, more experiments are required to achieve a fully quantitative interpretation of our data. A crucial point is to prepare molecularly smooth surfaces. The importance of thermal

motion might be evaluated by studying particles of varying size. Increasing the density of binding sites might be useful to study interactions with ligand and receptor molecules with low kinetic constants of association. Finally, it would be interesting to compare the results obtained with the flow chamber with data obtained by studying the vertical motion of small particles approaching binding sites, when they are driven by thermal motion (as performed by Liebert and Prieve [44], who took advantage of total internal reflection microscopy to determine particle-surface distance) or adjustable ultra-low forces generated by inflatable vesicles (as performed by Evans *et al.* [45], who measured particle-surface distance with interference-reflexion microscopy).

Acknowledgments

This work was supported by a grant from the A.R.C.

References

[1] Von Andrian U. H., Chambers J. D., McEvoy L. M., Bargatze R. F., Arfors K. E. and Butcher E. C., Two-step model of leukocyte-endothelial cell interactions in inflammation: distinct roles for LECAM-1 and the leukocyte β2-integrins *in vivo*, *Proc. Nat. Acad. Sci. USA* **88** (1991) 7538-7542.

[2] Lawrence M. B. and Springer T. A., Leukocytes roll on a selectin at physiological flow rates: distinction from and prerequisite for adhesion through integrins, *Cell* **65** (1991) 859-873.

[3] Berlin C., Bargatze R. F., Campbell J. J., Von Andrian U. H., Szabo M. C., Hasslen S. R., Nelson R. D., Berg E. L., Erlandsen S. L. and Butcher E. C., Alpha 4 integrins mediate lymphocyte attachment and rolling under physiologic flow, *Cell* **80** (1995) 413-422

[4] Springer T. A., Traffic signals for lymphocyte recirculation and leukocyte emigration: the multi-step paradigm, *Cell* **76** (1994) 301-314.

[5] Bell G. I., Models for the specific adhesion of cells to cells, *Science* **200** (1978) 618-627.

[6] Bell G. I., Dembo M. and Bongrand P., Cell adhesion, Competition between nonspecific repulsion and specific bonding, *Biophys. J.* **45** (1984) 1051-1064.

[7] Evans E. A., Detailed mechanics of membrane-membrane adhesion and separation. I Continuum of molecular cross-bridges, *Biophys. J.* **48** (1985) 175-183.

[8] Hammer D. A. and Lauffenburger D. A., A dynamical model for receptor-mediated cell adhesion to surfaces, *Biophys. J.* **52** (1987) 475-487.

[9] Dembo M., Torney D. C., Saxman K. and Hammer D., The reaction-limited kinetics of membrane to surface adhesion and detachment, *Proc. Roy. Soc. Lond B.* **234** (1988) 55-83.

[10] Hammer D. A. and Apte S. M., Simulation of cell rolling and adhesion on surfaces in shear flow: general results and analysis of selectin-mediated neutrophil adhesion, *Biophys. J.* **63** (1992) 35-57.

[11] Tözeren A. and Ley K., How do selectins mediate leukocyte rolling in venules, *Biophys J.* **63** (1992) 700-709.

[12] Evans E. A., Detailed mechanics of membrane-membrane adhesion and separation. II. Discrete kinetically trapped molecular cross-bridges, *Biophys. J.* **48** (1985) 185-192.

[13] Cozens-Roberts C., Lauffenburger D. A. and Quinn J. A., Receptor-mediated cell attachment and detachment kinetics. I - Probabilistic model and analysis, *Biophys. J.* **58** (1990) 841-856.

[14] van der Merwe P. A., Brown M. H., Davis S. J. and Barclay A. N., Affinity and kinetic analysis of the interaction of the cell adhesion molecules rat CD2 and CD48, *EMBO J.* **12** (1993) 4945-4954.

[15] Nelson R.M., Venot A., Bevilacqua M.P., Linhardt R.J. and Stamenkovic I., Carbohydrate-protein interactions in vascular biology, *Ann. Rev. Cell Biol.* **11** (1995) 601-631.

[16] Brenner H., The slow motion of a sphere through a viscous fluid towards a plane surface, *Chem. Eng. Sci.* **16** (1961) 242-251.

[17] Goldmann A. J., Cox R. G. and Brenner H., Slow viscous motion of a sphere parallel to a plane wall - II - Couette flow, *Chem. Eng. Sci.* **22** (1967) 653-660.

[18] Happel J. and Brenner H., Low Reynolds Number Hydrodynamics, 2nd Ed. (Kluwer Academic Publishers, Dordrecht, 1973) pp. 322-331.

[19] Prieve D. C. and Alexander B. M., Hydrodynamic measurement of double-layer repulsion between colloidal particle and flat plate, *Science* **231** (1986) 1269-1270.

[20] Doroszewski J., Skierski J. and Przadka L., Interactions of neoplastic cells with glass surface under flow conditions, *Exp. Cell Res.* **104** (1977) 335-343.

[21] Forrester J. V. and Lackie J. M., Adhesion of neutrophil leucocytes under conditions of flow, *J. Cell Sci.* **70** (1984) 93-110.

[22] Mège J. L., Capo C., Benoliel A. M. and Bongrand P., Determination of binding strength and kinetics of binding initiation - A model study made on the adhesive properties of P388D1 macrophage-like cells, *Cell Biophys.* **8** (1986) 141-160.

[23] Tissot O., Foa C., Capo C., Brailly H., Delaage M. and Bongrand P., Influence of adhesive bonds and surface rugosity on the interaction between rat thymocytes and flat surface under laminar shear flow, *J. Disp. Sci. & Technology* **12** (1991) 145-160.

[24] Pierres A., Tissot O., Malissen B. and Bongrand P., Dynamic adhesion of CD8-positive cells to antibody-coated surfaces: the initial step is independent of microfilaments and intracellular domains of cell binding molecules, *J. Cell Biol.* **125** (1994) 945-953.

[25] Tempelman L. A. and Hammer D. A., Receptor-mediated binding of IgE-sensitized rat basophilic leukemia cells to antigen-coated substrates under hydrodynamic flow, *Biophys. J.* **66** (1994) 1231-1243.

[26] Alon R., Hammer D. A. and Springer T. A., Lifetime of the P-selectin-carbohydrate bond and its response to tensile force in hydrodynamic flow, *Nature* **374** (1995) 539-542.

[27] Wattenbarger M. R., Graves D. J. and Lauffenburger D. A., Specific adhesion of glycophorin liposomes to a lectin surface in shear flow, *Biophys. J.* **57** (1990) 765-777.

[28] Pierres A., Benoliel A. M. and Bongrand P., Measuring the lifetimes of bonds made between surface-linked molecules, *J. Biol. Chem.* **270** (1995) 26586-26592.

[29] Lawrence M. B., Smith C. W., Eskin S. G. and McIntire L. V., Effect of venous shear stress on CD18-mediated neutrophil adhesion to cultured endothelium, *Blood* **75** (1990) 227-237.

[30] Kaplanski G., Farnarier C., Tissot O., Pierres A., Benoliel A. M., Alessi M. C., Kaplanski S. and Bongrand P., Granulocyte-endothelium initial adhesion: analysis of transient binding events mediated by E-selectin in a laminar shear flow, *Biophys. J.* **64** (1993) 1922-1933.

[31] Xia Z., Goldsmith H. L. and van de Ven T. G. M., Kinetics of specific and nonspecific adhesion of red blood cells on glass, *Biophys. J.* **65** (1993) 1073-1083.

[32] Tempelman L. A., Park S. and Hammer D. A., Motion of model leukocytes near a wall in simple shear flow: deviation from hard sphere theory, *Biotechnology Progress* **10** (1994) 97-108.

[33] Tissot O., Pierres A., Foac C., Delaage M. and Bongrand P., Motion of cells sedimenting on a solid surface in a laminar shear flow, *Biophys. J.* **61** (1992) 204-215.

[34] Tissot O., Pierres A., and Bongrand P. in Studying Cell Adhesion, P. Bongrand, P. M. Claesson & A. Curtis, Eds (Springer, Heidelberg, 1994) pp. 157-174.

[35] Pierres A., Benoliel A.M. and Bongrand P., Use of thermal fluctuations to study the length and flexibility of ligand-receptor bonds, *C. R. Acad. Sci. Paris* **318** (1995) 1191-1196.

[36] André P., Benoliel A.M., Capo C., Foa C., Buferne M., Boyer C., Schmitt-Verhulst A.M. and Bongrand P., Use of conjugates made between a cytolytic T cell clone and target cells to study the redistribution of membrane molecules in cell contact areas, *J. Cell Sci.* **97** (1990) 335-347.

[37] Goldman A. J., Cox R. G. and Brenner H., Slow viscous motion of a sphere parallel to a plane wall - I - Motion through a quiescent fluid, *Chem. Engn. Sci.* **22** (1967) 637-651.

[38] Tha S. P., Shuster J. and Goldsmith H. L., Interaction forces between red cells agglutinated by antibody. II. Measurement of hydrodynamic force of breakup, *Biophys. J.* **50** (1986) 1117-1126.

[39] Evans E. A., Berk D. and Leung A. Detachment of agglutinin-bonded red blood cells. I - Forces to rupture molecular-point attachment, *Biophys J.* **59** (1991) 838-848.

[40] Florin E. L., Moy V. T. and Gaub H. E., Adhesion forces between individual ligand-receptor pairs, *Science* **264** (1994) 415-417.

[41] Valentine R. C. and Green N. M., Electron microscopy of an antibody-hapten complex, *J. Mol. Biol.* **27** (1967) 615-617.

[42] Uyeda T. Q. P., Warrick, H. M., Kron, S. J. and Spudich J. A., Quantized velocities at low myosin densities in an *in vitro* motility assay, *Nature* **352** (1991) 307-311.

[43] Bongrand P. and Bell G. I., Cell-cell adhesion: parameters and possible mechanisms. In "Cell Surface Dynamics: concepts and models", A. S. Perelson, C. DeLisi and F. W. Wiegel, Eds. (Marcel Dekker inc., 1984) pp. 459-493.

[44] Liebert R. B. and Prieve D. C., Species-specific long range interactions between receptor/ligand pairs, *Biophys. J.* **69** (1995) 66-73.

[45] Evans E. A., Ritchie K. and Merkel R., Sensitive force technique to probe molecular adhesion and structural linkages at biological interfaces, *Biophys. J.* **68** (1995) 2580-2587.

Commission paritaire N° 57920

 Directrice de la Publication : Jeanne BERGER

SaisieTEX-LATEX : Les Éditions de Physique
Impression JOUVE, 18, rue Saint-Denis, 75001 PARIS
N° 236907X. Dépôt légal · Juin 1996